Integrated ionic liquid and rate-based absorption process design for gas separation: Global optimization using hybrid models

Xiang Zhang[1] | Xuechong Ding[2] | Zhen Song[2] | Teng Zhou[1,2] [ID] |
Kai Sundmacher[1,2] [ID]

[1]Process Systems Engineering, Max Planck Institute for Dynamics of Complex Technical Systems, Magdeburg, Germany

[2]Process Systems Engineering, Otto-von-Guericke University Magdeburg, Magdeburg, Germany

Correspondence
Teng Zhou, Process Systems Engineering, Max Planck Institute for Dynamics of Complex Technical Systems, Sandtorstr. 1, D-39106 Magdeburg, Germany.
Email: zhout@mpi-magdeburg.mpg.de

Funding information
Computer-Aided Material and Process Design (CAMPD) Ernst Dieter Gilles Postdoctoral Fellowship are funded by the Max Planck Society, Germany

Abstract

A new method for integrated ionic liquid (IL) and absorption process design is proposed where a rigorous rate-based process model is used to incorporate absorption thermodynamics and kinetics. Different types of models including group contribution models and thermodynamic models are employed to predict the process-relevant physical, kinetic, and thermodynamic (gas solubility) properties of ILs. Combining the property models with process models, the integrated IL and process design problem is formulated as an MINLP optimization problem. Unfortunately, due to the model complexity, the problem is prone to convergence failure. To lower the computational difficulty, tractable surrogate models are used to replace the complex thermodynamic models while maintaining the prediction accuracy. This provides an opportunity to find the global optimum for the integrated design problem. A pre-combustion carbon capture case study is provided to demonstrate the applicability of the method. The obtained global optimum saves 14.8% cost compared with the Selexol process.

KEYWORDS
absorption kinetics, carbon capture, computer-aided ionic liquid design, global optimization, rate-based absorption, surrogate modeling

1 | INTRODUCTION

Gas separation is an inevitable process in many industries. Several technologies such as absorption, adsorption, and membrane separation are available for gas separation. Among these existing technologies, solvent-based absorption is a mature and easy-to-operate one. Its industrial applications include carbon capture, natural gas sweetening, dehydration, and so on.[1] It is known that the core for employing absorption processes lies in the use of high-performing solvents, the search for new advanced solvents is essential to enhance the performance of absorption processes.[2]

Ionic liquids (ILs) are regarded as potential alternatives to organic solvents for gas separation due to their superior gas solubility, low volatility as well as chemical and thermal stability.[3,4] However, the number of ILs is almost infinite when considering the large number of anions, cations, and substituent groups. Clearly, using the traditional trial-and-error method is inefficient for selecting optimal ILs.[5] So far, many efforts have been made on computational IL screening. For the purpose of IL absorbent screening, various predictive models such as ab initio calculations, equations of state (EOS), and activity coefficient models (e.g., COSMO-RS) have been utilized to estimate the thermodynamic properties of ILs (mainly gas solubility).[5–9] Although these approaches can efficiently screen ILs with desired properties, they are limited by the number of available IL candidates in the databases. To further expand the

search space and find new promising ILs, a systematic approach for IL design is highly necessary.

Computer-aided design methods have been developed and successfully applied for both organic solvent design[10–13] and IL solvent design.[14–17] For computer-aided ionic liquid design (CAILD), an IL molecule is decomposed into different structural groups and its properties are calculated using quantitative structure–property relationship models (e.g., group contribution models). With these, the IL molecular structure is optimized to achieve desired properties through the formulation and solution of a mixed-integer optimization problem.[17] For predicting IL physical properties (e.g., melting point and boiling point), simple linear group contribution (GC) models are suitable and can be easily applied.[18–20] Besides, for predicting thermodynamic properties (e.g., activity coefficient and solubility) of IL systems, the nonlinear GC-based UNIFAC models are often used.[21,22] In order to make accurate predictions, the involved UNIFAC model parameters for IL systems have been extensively fitted from experimental data.[23,24]

No matter which type of solvent (organic or IL) is used, it ultimately serves a specific process and the process performance depends on the solvent selection and process operations.[25] Given the strong interdependency between these two issues, integrated solvent and process design is always preferred for enhancing the overall process efficiency.[26–28] For absorption processes, the left of Figure 1 shows that such an integrated design problem needs to consider the variations at the interlinked molecular, phase, and process levels. In the literature, a few efforts have been made on the integrated solvent and absorption process design.[28–31] However, the existing studies only considered the absorption thermodynamics in the phase level so that relatively simple absorption process models can be applied. In fact, absorption kinetics can dominate over the thermodynamics. For instance, the key role of absorption kinetics over thermodynamics in IL selection for CO_2 capture has been revealed.[32–34] Ignoring kinetics can lead to sub-optimal or even poor solutions for absorption process development. To identify truly optimal solvent and absorption process, a rigorous rate-based absorption process model that incorporates absorption thermodynamics and kinetics should be used. In this work, a new computer-aided IL and process design (CAILPD) method

is developed based on the rigorous rate-based absorption process model where the effects of ILs on absorption thermodynamics and kinetics are simultaneously considered. This approach can theoretically provide a better and more comprehensive design on gas absorption processes.

Note that for a given solvent, the optimization of rigorous rate-based absorption processes has been studied.[35] However, no one has used the rate-based process model for integrated solvent and absorption process design. The main reason is that such design problems usually lead to challenging mixed-integer nonlinear programming (MINLP) problems, especially when complex thermodynamic models are used.[25,36] Thus, an efficient solution strategy is highly desired to solve the complex integrated design problems. Recently, surrogate models that are constructed from reliable data to substitute complicated physical models have been widely adopted in process optimization.[37,38] This can effectively lower the computational difficulty while maintaining the model reliability. Although surrogate modeling is not a new technique for process design, it is still not clear whether and how surrogate models should be used to solve integrated solvent and process design problems, particularly when multiple models can be substituted. Thus, it motivates us to properly incorporate surrogate model into the proposed CAILPD framework for achieving a convergence to global optimality that usually cannot be obtained otherwise. The article is organized as follows. First, the general CAILPD methodology and framework are introduced. Afterward, the CAILPD approach is applied and demonstrated on a pre-combustion carbon capture case study.

2 | COMPUTER-AIDED IONIC LIQUID AND PROCESS DESIGN METHODOLOGY BASED ON HYBRID MODELS

The proposed CAILPD methodology is illustrated in Figure 1. The absorption system contains three interlinked levels: molecular, phase, and process. The design variables consist of IL molecular structures and process operating conditions which together affect the absorption kinetics and thermodynamics. The rate-based absorption process
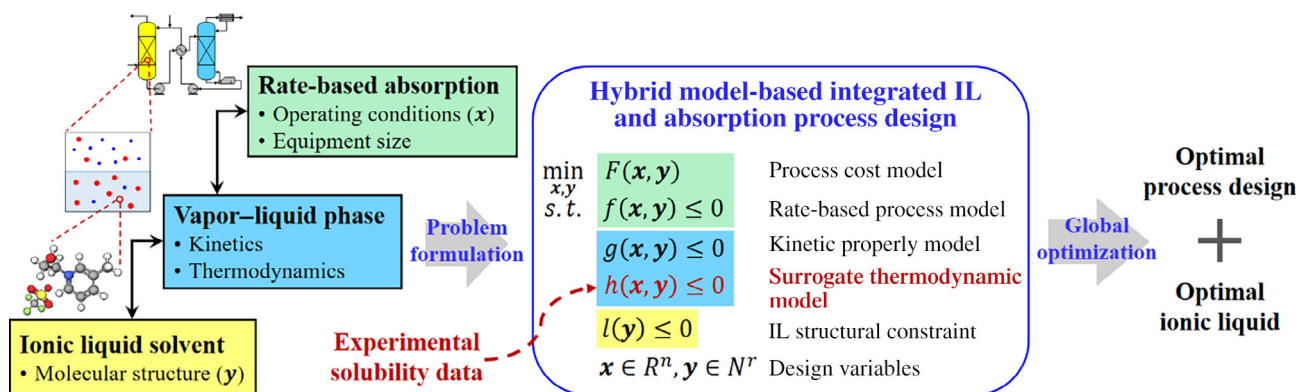

FIGURE 1 The General CAILPD methodology based on hybrid models

model is used to capture both effects. In addition, the equipment sizes and process costs can be calculated. Such a multilevel design problem is formulated as an MINLP problem. The objective is to minimize the process cost while fulfilling multiple constraints. Traditionally, the thermodynamic property (i.e., equilibrium gas solubility) is calculated by GC-based predictive models such as UNIFAC-IL and Peng–Robinson (PR).[9,39] Our idea is to construct a mathematically simple but reliable surrogate model for predicting the gas solubility based on existing experimental data. Along with other physical models, a hybrid model-based design formulation is formed. This enables us to pursue global optimization of the resulting MINLP problem, which can provide a better and more comprehensive absorption process design. The detailed modeling framework is described below. Note that both the two treatments of thermodynamics are included for better comparison and demonstration of the advances of our proposed method.

3 | COMPUTER-AIDED IONIC LIQUID AND PROCESS DESIGN MODELING FRAMEWORK

Figure 2 shows the modeling framework for computer-aided ionic liquid and rate-based absorption process design. The design problem can be decomposed into two main steps, a forward prediction or simulation step (blue solid lines) and a reverse design or optimization step (red dash lines). The forward step relates IL molecular structure and process operating conditions with the final process performance via different types of models. As illustrated, the effects of ILs on the mass transfer coefficient of absorption are quantified by employing QSPR or group contribution (GC) models and certain correlation equations. On the other hand, gas fugacity and activity coefficients in the vapor and liquid phases can be predicted by traditional thermodynamic models and the equilibrium gas solubility is then calculated through the solution of the vapor–liquid equilibrium (VLE) equation. Alternatively, the thermodynamic equilibrium solubility can be directly predicted by surrogate models. Substituting the mass transfer coefficient and thermodynamic driving force into the rate-based absorption model, the corresponding process performance can thus be evaluated for a given IL and process condition. After completing the forward step, the best IL structure and optimal process conditions can be

reversely identified by solving an MINLP problem where the process performance is optimized considering all the models or equations as well as IL structural constraints. The proposed method and framework are illustrated using a pre-combustion carbon capture example.

4 | COMPUTER-AIDED IONIC LIQUID AND PROCESS DESIGN FOR PRE-COMBUSTION CARBON CAPTURE

4.1 | Representation of ionic liquids

The first step for designing ILs is to decompose them into different building blocks. ILs can be represented in different ways. In this work, an IL is decomposed into an anion, a cation core, and substituents linked to the cation core. This representation can provide large design space and flexibility.[40] Taking 1-propyl-3-methylimidazolium bis(trifluoromethylsulfonyl)imide [C_3mim][Tf_2N] as an example (see Figure 3), this IL is constituted by an anion "Tf_2N," a cation core "MIm," and 3 substituent groups including 1 "aN_CH_2," 1 "CH_2," and 1 "CH_3."

In the present work, 23 anions, 12 cation cores, and 17 cation substituent groups are considered for the IL design, as listed in Table 1. Each generated IL is denoted by a vector $n = [n_1,...,n_i,...,n_N]$ where $N = 52$ and the element n_i represents the number of the ith building group presented in the IL molecule. Note that only the

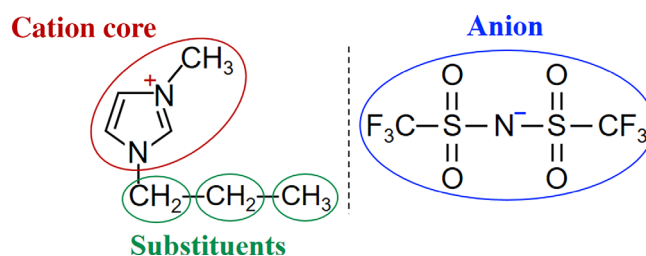

FIGURE 3 Representation of building groups of ionic liquids exemplified for [C_3mim][Tf_2N]
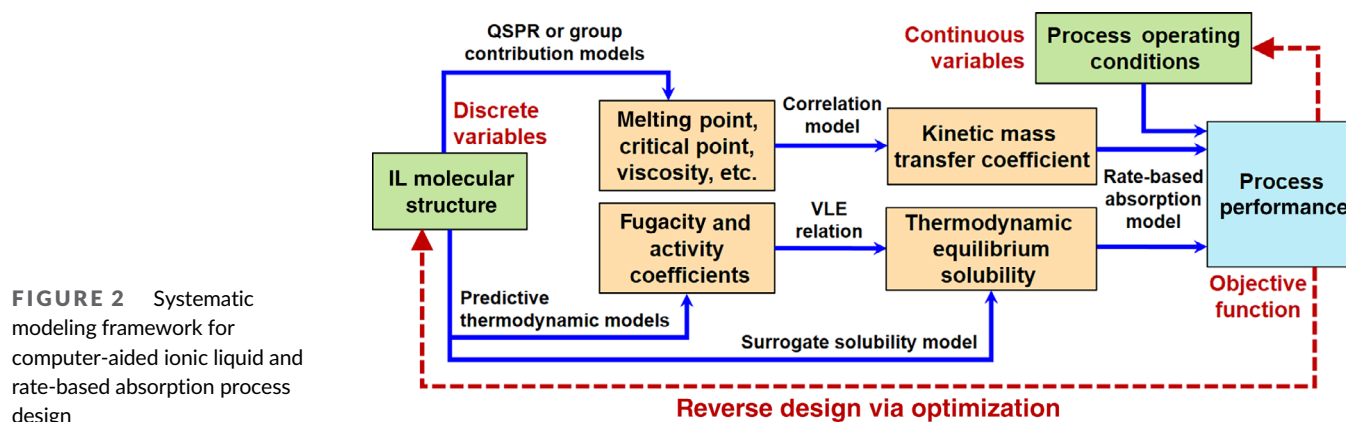

FIGURE 2 Systematic modeling framework for computer-aided ionic liquid and rate-based absorption process design

TABLE 1 Anions, cations, and cation substituent groups considered for IL design

Anions (G_{anion})	BF_4, Cl, DCA, NO_3, PF_6, SCN, $C(CN)_3$, HSO_4, Tf_2N, BETA, FOR, TFA, $C_3F_7CO_2$, $MeSO_4$, $EtSO_4$, $MDEGSO_4$, $MeSO_3$, TfO, NfO, TDfO, TOS, $C_{12}H_{25}PhSO_3$, methide
Cations (G_{cation})	Im13, MIm, MMIM, Py, MPyrro, MPy, MPip, NH_3, NH_2, NH, N, P
Substituents (G_{sub})	CH_3, N_CH_3, P_CH_3, aN_CH_3, $cycN\_CH_3$, CH_2, N_CH_2, P_CH_2, aN_CH_2, $cycN\_CH_2$, CH, N_CH, OCH_2, OCH_3, CF_2, CF_3, OH

TABLE 2 Classification of cation substituent groups

Alkyl group (G_{ag})	CH_3, N_CH_3, P_CH_3, aN_CH_3, $cycN\_CH_3$, CH_2, N_CH_2, P_CH_2, aN_CH_2, $cycN\_CH_2$, CH, N_CH
Non-CH_3 alkyl group (G_{nCH_3})	CH_2, N_CH_2, P_CH_2, aN_CH_2, $cycN\_CH_2$, CH, N_CH
Functional group (G_{fg})	OCH_2, OCH_3, OH, CF_2, CF_3
Ether and hydroxyl group (G_{eh})	OCH_2, OCH_3, OH
Fluorized alkyl group (G_{fag})	CF_2, CF_3
Alkyl group linked to aromatic nitrogen (G_{aN})	aN_CH_3, aN_CH_2
Alkyl group linked to cyclic nitrogen (G_{cycN})	$cycN\_CH_3$, $cycN\_CH_2$
Alkyl group linked to acyclic nitrogen (G_N)	N_CH_3, N_CH_2, N_CH
Alkyl group linked to acyclic phosphorous (G_P)	P_CH_3, P_CH_2
CH_3 group directly linked to cation (G_{DCH_3})	N_CH_3, P_CH_3, aN_CH_3, $cycN\_CH_3$
Group not directly linked to cation (G_{NDC})	CH_3, CH_2, CH, OCH_2, OCH_3, CF_2, CF_3, OH

abbreviations of groups are given and their molecular structures are shown in Table S1. In addition, their contributions to properties (e.g., molecular weight, melting point, etc.) and the upper bounds in the CAILPD program are listed in Table S1 as well. These contributions are considered as parameters in the following sections. Note that the nomenclature is presented at the end of the Appendix S1.

4.2 | Ionic liquids structural constraints

To generate a feasible IL, certain structural constraints must be satisfied. A feasible IL consists of only one anion and one cation (Equations 1 and 2). Equation (3) shows that the number of each constituent group should be non-negative and less than its upper bound n_i^{upp}. The total number of constituent groups including cation, anion, and substituent groups is between 2 and 8.

$$\sum_{i \in G_{anion}} n_i = 1 \tag{1}$$

$$\sum_{i \in G_{cation}} n_i = 1 \tag{2}$$

$$0 \le n_i \le n_i^{upp} \quad \forall i \in G_{tot} \tag{3}$$

$$2 \le \sum_{i \in G_{tot}} n_i \le 8, \ G_{tot} = \{G_{cation}, G_{anion}, G_{sub}\} \tag{4}$$

Since cation substituents in a normal IL are acyclic, the simple octet rule in Equation (5) ensures that an IL has zero valency. PVA_i is the valency of the ith constituent group. Note that when monocyclic or bicyclic cation substituents are open for consideration, a more general formulation can be derived from Ref. 41. The modified bonding rule in Equation (6) ensures that two adjacent groups in an IL are not linked by more than one bond.

$$\sum_{i \in G_{cation} \cup G_{sub}} n_i \cdot (2 - PVA_i) = 2 \cdot q, \ q = 1 \text{ for acyclic cation substituents} \tag{5}$$

$$n_i \cdot (PVA_i - 1) + 2 \le \sum_{j \in G_{cation} \cup G_{sub}} n_j, \ \forall i \in \{G_{cation}, G_{sub}\} \tag{6}$$

Based on the chemical intuitions, two functional groups are generally not linked to one single carbon atom. Thus, Equation (7) means that the total number of functional substituent groups is no more than that of the alkyl substituent groups. G_{fg} and G_{ag} are the sets of functional and alkyl substituent groups, respectively. The detailed classification of cation substituent groups are given in Table 2.

$$\sum_{i \in G_{fg}} n_i \le \sum_{j \in G_{ag}} n_j \tag{7}$$

Considering the structural characteristics of normal ILs, the structural complexity of ILs is refined using Equations (8)–(11). Equations (8) and (9) ensure that the total number of ether and hydroxyl groups (G_{eh}) is less than 2 and less than the total number of non-CH_3 alkyl groups (G_{nCH_3}), respectively. In addition, the total number of fluorized alkyl groups (G_{fag}) is less than 2 (Equation 10). Ether and hydroxyl groups and fluorized alkyl groups cannot exist simultaneously (Equation 11).

$$\sum_{i \in G_{eh}} n_i \le 2 \tag{8}$$

$$\sum_{i \in G_{eh}} n_i \le \sum_{j \in G_{nCH_3}} n_j \tag{9}$$

$$\sum_{i \in G_{fag}} n_i \le 2 \tag{10}$$

$$\sum_{i \in G_{eh}} n_i \cdot \sum_{j \in G_{fag}} n_j = 0 \tag{11}$$

Equations (12)–(16) ensure that the cation is properly linked to the corresponding substituent groups. G_{aN} and G_{cycN} are the sets of alkyl groups linked to the aromatic and cyclic nitrogen, respectively. G_N and G_P are the alkyl groups linked to acyclic nitrogen and acyclic phosphorous, respectively. Based on the cation structures (Table S1), any alkyl group linked to Im13, MIm, MMIM, Py, or MPy is directly linked to an aromatic nitrogen. With this, the set G_{aN} is defined. In addition, the first part of Equation (12) ensures that if any of these cations is selected, some alkyl groups in G_{aN} should be selected and the number of the selected G_{aN} groups must match the cation valency. Meanwhile, Equation (13) ensures that the alkyl groups in the other sets (i.e., G_{cycN}, G_N, and G_P) are not selected. On a similar manner, the other parts of Equation (12) and Equations (14)–(16) are proposed.

$$\left(\frac{n_{Im13}}{2} + n_{MIm} + n_{MMIM} + n_{Py} + n_{MPy}\right) \cdot \sum_{i \in G_{aN}} n_i + \left(n_{MPyrro} + n_{MPip}\right) \cdot \sum_{i \in G_{cycN}} n_i$$
$$+ \left(\frac{n_N}{4} + \frac{n_{NH}}{3} + \frac{n_{NH_2}}{2} + n_{NH_3}\right) \cdot \sum_{i \in G_N} n_i + \frac{n_P}{4} \cdot \sum_{i \in G_P} n_i = 1 \tag{12}$$

$$\left(n_{Im13} + n_{MIm} + n_{MMIM} + n_{Py} + n_{MPy}\right) \cdot \left(\sum_{i \in G_{cycN}} n_i + \sum_{i \in G_N} n_i + \sum_{i \in G_P} n_i\right) = 0 \tag{13}$$

$$\left(n_{MPyrro} + n_{MPip}\right) \cdot \left(\sum_{i \in G_{aN}} n_i + \sum_{i \in G_N} n_i + \sum_{i \in G_P} n_i\right) = 0 \tag{14}$$

$$\left(n_N + n_{NH} + n_{NH_2} + n_{NH_3}\right) \cdot \left(\sum_{i \in G_{cycN}} n_i + \sum_{i \in G_{aN}} n_i + \sum_{i \in G_P} n_i\right) = 0 \tag{15}$$

$$n_P \cdot \left(\sum_{i \in G_{cycN}} n_i + \sum_{i \in G_{aN}} n_i + \sum_{i \in G_N} n_i\right) = 0 \tag{16}$$

Equations (17)–(20) ensure that if the cation is only linked to CH3, no other substituent groups can exist. G_{DCH_3} and G_{NDC} are the sets of CH$_3$ group directly linked to cation and group not directly linked to cation, respectively. For instance, the valency of MIm, MMIM, Py, MPy, MPyrro, MPip, and NH$_3$ are equal to 1. Clearly, at most one CH$_3$ group can directly be linked to these cations and no other groups from the set G_{NDC} can exist. This rule is formulated as Equation (17). Similarly, Equations (18)–(20) are developed for the cations with a valency of 2, 3, and 4, respectively.

$$\left(n_{MIm} + n_{MMIM} + n_{Py} + n_{MPy} + n_{MPyrro} + n_{MPip} + n_{NH_3}\right) \cdot \left(0 - \sum_{i \in G_{DCH_3}} n_i\right) \cdot \sum_{j \in G_{NDC}} n_j \geq 0 \tag{17}$$

$$\left(n_{Im13} + n_{NH_2}\right) \cdot \left(1 - \sum_{i \in G_{DCH_3}} n_i\right) \cdot \sum_{j \in G_{NDC}} n_j \geq 0 \tag{18}$$

$$n_{NH} \cdot \left(2 - \sum_{i \in G_{DCH_3}} n_i\right) \cdot \sum_{j \in G_{NDC}} n_j \geq 0 \tag{19}$$

$$\left(n_N + n_P\right) \cdot \left(3 - \sum_{i \in G_{DCH_3}} n_i\right) \cdot \sum_{j \in G_{NDC}} n_j \geq 0 \tag{20}$$

4.3 | Ionic liquid physical and kinetic property prediction

Physical and kinetic properties of ILs are required for the rate-based process modeling. Figure 4 summarizes different models for predicting the physical and kinetic properties of ILs. The detailed model descriptions are elaborated below.

4.3.1 | Group contribution models to physical properties

The molecular weight (MW), melting point (T_m), and boiling point (T_b) of ILs are calculated using the GC methods in Equations (21)–(23).[42,43] PMW_i, PTm_i, and PTb_i are the contributions of the ith group to the corresponding properties (see Table S1).
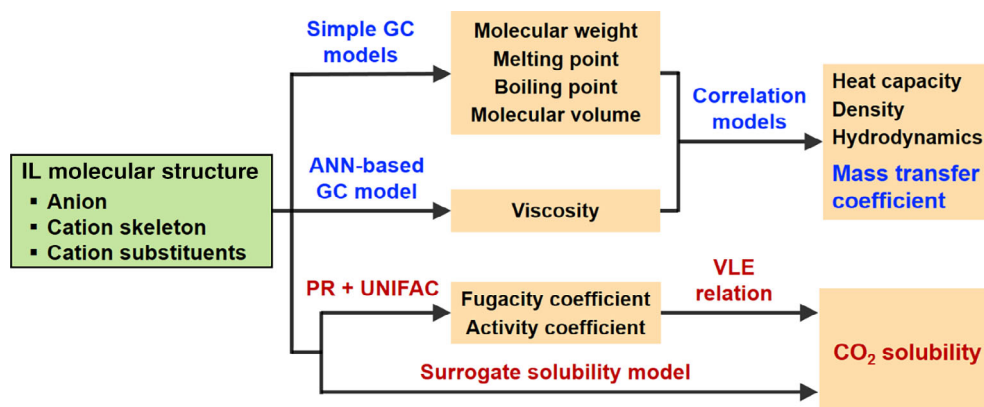

FIGURE 4 Models for predicting the physical and kinetic properties of ionic liquids

$$MW = \sum_{i \in G_{tot}} n_i \cdot PMW_i \qquad (21)$$

$$T_m = 288.7 + \sum_{i \in G_{tot}} n_i \cdot PTm_i \qquad (22)$$

$$T_b = 198.2 + \sum_{i \in G_{tot}} n_i \cdot PTb_i \qquad (23)$$

IL molar volume (MV) depends on the temperature (T) and pressure (P) in Equation (24). The molar volume (MV_0) at $T_0 = 298.15\,K$ and $P_0 = 1.0\,bar$ is calculated using the GC approach in Equation (25). PMV_i is the ith group's contribution to molar volume (see Table S1).[44]

$$MV = MV_0 \cdot \left[1 + \frac{6.439(T - T_0)}{10,000}\right]$$
$$\cdot \left[1 - 0.081 \times \ln\left(1 + \frac{(1 + 0.00497[T - T_0])(P - P_0)}{1950}\right)\right] \qquad (24)$$

$$MV_0 = \sum_{i \in G_{tot}} n_i \cdot PMV_i \qquad (25)$$

An artificial neural network (ANN) based GC model has been developed to predict IL viscosity.[45] The model consists of three layers (i.e., input layer, hidden layer, and output layer). Based on the ANN-GC model, the viscosity (μ) of ILs can be expressed as

$$\mu = f_{ANN-GC}(n_i, T, P) \qquad (26)$$

The detailed model equations are given in Appendix S2.

4.3.2 | Correlation models to physical and kinetic properties

The density (ρ) and heat capacity (C_p) of ILs are calculated using the following correlation functions.[43,46]

$$\rho = \frac{1000 \times MW}{MV} \qquad (27)$$

$$C_p = \frac{7.7 + 0.226(T - 298.15) + 1.918MV}{MW} \qquad (28)$$

Moreover, when ILs are used for CO_2 absorption in a packed column, it can be assumed that mass transfer resistance occurs in the vicinity of gas–liquid interface. With this, the mass transfer coefficient (k) can be estimated using the Onda' correlation.[47,48]

$$k \left(\frac{\rho}{1000 \times \mu \cdot g}\right)^{\frac{1}{3}} = 0.000051 \times Re_w^{\frac{2}{3}} \cdot (a_p \cdot d_p)^{0.4} \cdot Sc^{-0.5} \qquad (29)$$

where, g is the gravity constant. a_p and d_p are the specific packing surface area and diameter, respectively. Sc and D_{mass} are the Schmidt number and the mass diffusivity coefficient, respectively. The detailed models to calculate these two variables are given in Appendix S2.

4.4 | CO_2 solubility in ionic liquids

4.4.1 | Rigorous thermodynamic model

Based on thermodynamics, the vapor–liquid equilibrium (VLE) of CO_2 determines its solubility in ILs. At equilibrium, the molar fraction of CO_2 in ILs ($x_{CO_2}^{eq}$) can be expressed as

$$x_{CO_2}^{eq} = \frac{\varphi_{CO_2} \cdot y_{CO_2} \cdot P}{\gamma_{CO_2} \cdot Psat_{CO_2}} \qquad (30)$$

$$Psat_{CO_2} = 10 \times e^{\left(12.3312 - \frac{4759.46}{T + 156.462}\right)} \qquad (31)$$

$$\varphi_{CO_2} = f_{PR}(y_j, T, P) \qquad (32)$$

$$\gamma_{CO_2} = f_{UNIFAC-IL}\left(n_i, x_j^{eq}, T\right) \qquad (33)$$

where, y_{CO_2} is the molar fraction of CO_2 in the gas phase. $Psat_{CO_2}$ is the saturated pressure of CO_2 (in bar), estimated by the extrapolated Antoine equation in Equation (31). The fugacity coefficient φ_{CO_2} can be predicted using the PR model and the activity coefficient γ_{CO_2} can be calculated by the UNIFAC-IL model.[22] x_j^{eq} and y_j are the molar fraction of jth component in the liquid and gas phase, respectively.

4.4.2 | Artificial neural network-based solubility model

Alternatively, the CO_2 equilibrium solubility in ILs can be predicted by surrogate models. By using ANN and support vector machine algorithms, Song et al.[49] recently built two GC-based machine learning models to predict CO_2 equilibrium solubility in ILs. These two models were developed from a comprehensive database containing more than 10,000 CO_2 solubility data in various ILs at different temperatures and pressures. The mean absolute error and R^2 of the two models are less than 0.03 and larger than 0.97, respectively. These statistics indicate that the models can give reliable predictions on CO_2 equilibrium solubility. Moreover, according to the reported model errors, the ANN model is slightly better and thus is applied here. The ANN-GC model consists of a three-layer feed forward network. The input layer receives IL structure information and temperature and pressure. The hidden layer comprising of seven neurons transfers the input to the output layer where the CO_2 solubility is finally predicted. Specifically, the CO_2 equilibrium molar fraction $x_{CO_2}^{eq}$ is calculated by the following equations.

$$NN_t^1 = \sum_i NW_{t,i}^1 \cdot n_i + TW_t^1 \cdot T + PW_t^1 \cdot P \cdot y_{CO_2} + bW_t^1, t = 1, ..., 7 \quad (34)$$

$$NN_t^2 = 1 - \frac{2}{1 + e^{2 \times NN_t^1}} \quad (35)$$

$$x_{CO_2}^{eq} = \sum_{t=1}^{7} NW_t^2 \cdot NN_t^2 + bW^2 \quad (36)$$

where, the superscripts 1 and 2 denote the hidden layer and output layer, respectively. Subscripts t and i are the neuron and IL group indices, respectively. NW, TW, and PW are weighting factors to IL group numbers, temperature, and pressure, respectively. bW represents the bias. All these parameters can be found in Ref. 49.

4.5 | Ionic liquid-based absorption process model

Figure 5 illustrates the schematic diagram of IL-based absorption process for CO_2 capture. The feed gas is first compressed and cooled (if necessary) since high pressure and low temperature are favored for dissolving CO_2. Then, the compressed gas is fed to an absorber where it counter-currently contacts with the ILs. Meanwhile, CO_2 goes into the IL phase while other gases remain in the gas phase. The CO_2-rich ILs leave from the bottom of the absorber while the clean gas is collected from the top. Afterward, the CO_2-loaded ILs are heated and enter a flash tank which has a lower pressure than the absorber. In the flash tank, the captured CO_2 is released and collected. Later, the recovered ILs are cooled and sent back to the absorber. In addition, makeup ILs are added to the absorber in case of IL losses. The specific process models used for CAILPD are presented below. Note that only the models of absorber and flash tank that accounts for absorption and desorption, respectively are elaborated here. The models for compressor, heat exchangers, and pump are given in Appendix S2.

4.5.1 | Absorber

The rate-based model is used in the absorber. The column is presumably isothermal and T^{AB} should be larger than the melting temperature

to ensure that the ILs are in liquid. In addition, the column is divided into $NT = 20$ sections. In each section, the amount of CO_2 absorbed from gas to ILs (pern) is equal and decided from the mass balance.

$$T_m \leq T^{AB} \quad (37)$$

$$pern = \frac{M^{feed} \cdot y_{CO_2}^{feed} \cdot \theta}{NT} \quad (38)$$

where, $y_{CO_2}^{feed}$ and θ are the CO_2 molar fraction in the feed gas and the percentage of CO_2 to be absorbed, respectively. If the solubility of other gases in ILs is negligible, the liquid and vapor molar fractions of CO_2 in the nth section ($n = 1, ..., NT$ from the bottom up) can be calculated by

$$x_{n,CO_2} = \frac{M^{IL} x_{out,CO_2}^{FT} + (NT - n)pern}{M^{IL} + (NT - n)pern} \quad (39)$$

$$y_{n,CO_2} = \frac{M^{feed} y_{CO_2}^{feed} - n \times pern}{M^{feed} - n \times pern} \quad (40)$$

where, x_{out,CO_2}^{FT} is the molar fraction of CO_2 in the ILs regenerated from the flash tank (FT). In addition, the following summation equations must be satisfied for each section.

$$\sum_c x_{n,c} = 1 \quad (41)$$

$$\sum_c y_{n,c} = 1 \quad (42)$$

where, the subscript c denotes the gas and liquid components. Moreover, the height of the nth section (h_n) is calculated in Equation (43) and the height of the absorber H^{AB} is obtained by Equation (44).[48]

$$pern \cdot \frac{MV^{IL}}{10^6} = Void_p \cdot a_w \cdot CSA \cdot k \cdot h_n \cdot \left(\frac{x_{n,CO_2}^{eq}}{1 - x_{n,CO_2}^{eq}} - \frac{x_{n,CO_2}}{1 - x_{n,CO_2}} \right) \quad (43)$$
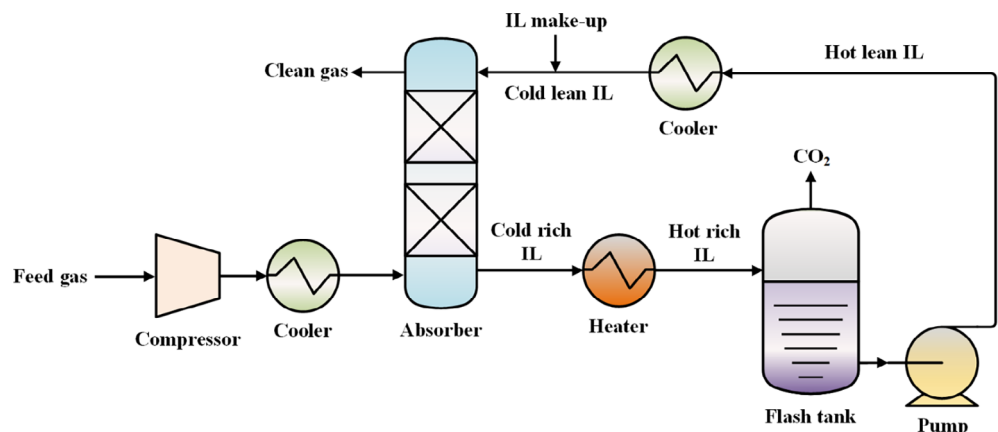
$$H^{AB} = \sum_{n=1}^{NT} h_n \quad (44)$$

FIGURE 5 Schematic diagram of IL-based absorption process for carbon capture

where, MV^{IL} denotes the molar volume of IL in the absorber (see Equations 24 and 25). $Void_p$ is the void fraction of packing. x^{eq}_{n,CO_2} represents the equilibrium CO_2 solubility in the nth column section. If rigorous thermodynamic models are used, it is calculated using Equations (30)–(33) with known y_{n,CO_2}. Alternatively, this equilibrium solubility can be directly calculated by Equations (34)–(36) if the ANN-based surrogate model is applied. In addition, Equation (45) ensures a positive driving force for CO_2 absorption.

$$x^{eq}_{n,CO_2} \geq x_{n,CO_2} \tag{45}$$

4.5.2 | Flash tank

The heated CO_2-loaded ILs are fed into the flash tank for solvent regeneration. The temperature in the flash tank cannot exceed the boiling point of IL to prevent its vaporization. The CO_2 molar fraction in the lean ILs x^{FT}_{out,CO_2} is estimated by the short-cut model in Equation (47).[50]

$$T^{FT} < T_b \tag{46}$$

$$x^{FT}_{out,CO_2} = 1 - \frac{1}{1 + \frac{P^{FT} \cdot MW}{10^4 \exp\left(6.8591 - \frac{2004.3}{T^{FT}}\right)}} \tag{47}$$

In order to facilitate the computation in the absorber, x^{FT}_{out,CO_2} is fixed to 0.02. In this case, the operating pressure of the flash tank P^{FT} depends on the temperature T^{FT}. Moreover, the flash tank is presumably operated on a half-full basis and the total volume of ILs in the flash tank is equal to the volume of 5 min IL flows.[51] Thus, the volume of the flash tank (V^{FT}) is expressed as

$$V^{FT} = 2 \times 300 \times M^{IL} \cdot \frac{MV^{FT}}{10^6} \tag{48}$$

where, MV^{FT} is the IL molar volume at T^{FT} and P^{FT}.

4.5.3 | Process economics

The performance of the IL-based carbon capture process is evaluated using the total annualized cost (TAC).

$$TAC = CRF \cdot C_{cap} + C_{ope} \tag{49}$$

$$C_{cap} = C^{COMP} + C^{GC} + C^{HE} + C^{CO} + C^{PUMP} + C^{AB} + C^{FT} \tag{50}$$

$$C_{ope} = C^{steam} + C^{ele} + C^{water} + C^{ml} \tag{51}$$

where, CRF is the capital recovery factor. C_{cap} is the summation of the capital costs of all the equipment. C_{ope} is the annual operating cost that accounts for the consumption of utilities (i.e., steam, electricity,

and cooling water) and other operating costs including labor, maintenance, and IL losses. The detailed calculation of the capital and operating costs is presented in Appendix S2.

5 | RESULTS AND DISCUSSION

As a major CO_2 emission resource, the pre-combustion flue gas is usually produced in an integrated gasification combined cycle (IGCC) based power plant. The feedstock such as natural gas is reacted with oxygen under high temperature and pressure to produce synthesis gas consisting of CO, H_2, and CO_2. Through a water-gas shift reaction, the CO is converted into CO_2 and the pre-combustion flue gas comprising mainly H_2 and CO_2 is formed. The CO_2 must be removed from the H_2 before power generation. In this work, the CAILPD framework is applied for pre-combustion carbon capture. The flue gas is assumed to be at 313.15 K and 20 bar with a molar flowrate of 10 kmol/s. The compositions of CO_2 and H_2 are set to 0.4 and 0.6, respectively. With an assumption that H_2 is not soluble in the ILs, the goal is to design a cost-effective IL-based absorption process for capturing no less than 90% CO_2 from the flue gas.

5.1 | First trail using rigorous thermodynamic model

In the first trial, the CAILPD problem is formulated using the classic thermodynamic models (i.e., UNIFAC and PR models) to predict the CO_2 equilibrium solubility. An MINLP problem is formed and summarized below. The objective is to minimize the process TAC while fulfilling the carbon capture requirement stated above. The design variables (degrees of freedom) consist of the discrete variable n_i and the continuous variables P^{AB} and T^{FT}. Equality constraints include IL structural constraints, property and process models as well as process economics. The specific feed gas conditions as well as process and costing parameters are listed in Table 3. The UNIFAC model parameters for the CO_2-IL systems can be found in Zhou et al.[24]

$$\min_{n_i, P^{AB}, T^{FT}} TAC$$

s.t. Equations (1)–(20)	IL structural constraints
Equations (21)–(33), (SA1)–(SA12)	IL property models
Equations (37)–(45)	Absorption model
Equations (46)–(48), (SB1)–(SB12)	Other process models
Equations (49)–(51), (SB13)–(SB27)	Process economics

The optimization problem is coded in GAMS 24.2 and solved using the deterministic global optimization solver BARON version 19.3.24.[52] The computational statistics are listed in the second column of Table 4. As shown, in total 52 discrete variables, 3086 single variables, 3121 equations, and 58,032 nonlinear matrix entries are involved. Clearly, this is a very complicated optimization problem.

TABLE 3 Input parameters for the pre-combustion carbon capture process

Input parameters for pre-combustion flue gas			
Gas composition			
CO_2	0.4	Temperature (K)	313.15
H_2	0.6	Pressure (bar)	20
Input molar flowrate (kmol/s)	10	Molar volume (L/mol)	1.28
Density (kg/m^3)	16.92	Heat capacity (kJ/kg/K)	1.72
Input parameters for the rate-based absorption process			
Inlet water temperature (K)	287	Hot steam temperature (K)	393.15
Outlet water temperature (K)	297	Steam latent heat (kJ/kg)	2201.6
Water heat capacity (kJ/kg/K)	4.18	Molar flowrate of IL (kmol/s)	3.75
Absorber temperature (K)	300	IL surface tension (N/m)	0.05
Absorber diameter (m)	5	IL association factor	0.14
Absorber thickness (m)	0.02	Packing surface area (m^2/m^3)	102
Packing diameter (m)	0.05	Packing void fraction	0.98
Flash tank thickness (m)	0.02	Packing critical surface tension (N/m)	0.075
CO_2 molar fraction in lean ILs	0.02	Flash tank diameter (m)	2.5
Isentropic coefficient	1.37	Partial molar volume of CO_2 in IL solutions (cm^3/mol)	34
Input parameters for process costing			
Capital recovery factor	0.1102	Reference cost of compressor (k$)	4714
Density of steel (kg/m^3)	7870	Reference work of compressor (kW)	22,371
Cooling water price ($/ton)	0.0316	Reference cost of heat exchanger (k$)	438
Steam price ($/kg)	0.0042	Reference area of heat exchanger (m^2)	1115
Electricity price ($/kWh)	0.0775	Reference cost of pump (k$)	420.1
IL price ($/kg)	10	Reference work of pump (m^3/s)	8.2

Different initial estimates and different ways of formulating equations are considered. However, it cannot converge within 24 h on a standard computer.

5.2 | Second trail using artificial neural network-based solubility model

In order to mitigate the computational difficulties, the highly complex thermodynamic models are replaced by the relatively simple ANN-based surrogate model. Furthermore, Equation (52) serves as an upper bound that limits the CO_2 equilibrium solubility at a specific absorption condition lower than 0.5. This absorption condition corresponds to the case where the feed gas is cooled and directly fed into the absorber. This constraint ensures that the ANN model does not extrapolate to unreasonable predictions.

$$x_{CO_2}^{eq*} = F_{ANN}\left(n_i, T = T^{AB}, P = 20\,\text{bar}, y_{CO_2} = 0.4\right) \leq 0.5 \quad (52)$$

F_{ANN} represents Equations (34)–(36). Replacing Equations (30)–(33) in the previous MINLP problem with Equations (34)–(36) and adding Equation (52) as an extra constraint, we can formulate another MINLP problem. The new optimization problem is solved with the global solver BARON as

TABLE 4 Computational statistics for the deterministic global optimization of the CAILPD problem

	UNIFAC-PR based models	ANN-based hybrid models
Solver	BARON	BARON
Number of discrete variables	52	52
Number of single variables	3086	439
Number of equations	3121	456
Number of nonlinear matrix entries	58,032	574
Computational time	No convergence within 24 h	5216 s

well. The third column of Table 4 lists the corresponding computational statistics. It consists of 52 discrete variables, 439 single variables, 456 equations, and 574 nonlinear matrix entries. It is clear that the problem size and nonlinearity are much less than those of the previous problem. It takes around 1.5 h for BARON to converge to the global optimality.

The obtained optimal IL and its properties as well as the operating conditions and process specifications are summarized in

Optimal IL group combination Optimal IL structure	2 CH₃, 2 N_CH₂, 1 OCH₂, 1 NH₂, 1 BETA

Flash tank temperature (K)	334.9
Absorber pressure (bar)	21.5
Absorber height (m)	19.4
CO_2 average solubility in the absorber	0.458
IL heat capacity in the absorber (J/g/K)	1.29
IL viscosity in the absorber (mPa s)	10.3
CO_2 mass transfer coefficient (m/s)	1.23×10^{-4}
Gas-cooling heat exchanger area (m²)	2090.0
IL-heating heat exchanger area (m²)	1187.7
IL-cooling heat exchanger area (m²)	3790.8
Cooling water consumption (ton/s)	2.17
Steam consumption (kg/s)	37.9
Compressor workload (kW)	1862.1
Pump workload (kW)	2530.3
Electricity consumption (kWh/s)	1.22
TAC (M\$/year)	11.44

TABLE 6 Top three ILs with their minimal total annualized cost

No.	IL group combination	TAC (m\$/year)
1	2 CH₃, 2 N_CH₂, 1 OCH₂, 1NH₂, 1 BETA	11.44
2	1 CH₃, 2 N_CH₂, 1 OH, 1NH₂, 1 BETA	12.42
3	1 N_CH₃, 1 CH₂, 1 N_CH₂, 1 OCH₂, 1 OH, 1 NH₂, 1 BETA	13.20

FIGURE 6 Cost breakdown of the optimal IL-based and DEPG-based absorption processes

Table 5. The corresponding minimized process *TAC* is 11.44 M $/year. The optimal IL found is *N*-ethyl-*N*-ethoxymethyl-ammonium bis(pentafluoroethanesulfonyl)amide [EEOMA][BETA] or *N*-ethyl-*N*-methoxyethyl-ammonium bis(pentafluoroethanesulfonyl)amide [EMOEA][BETA] that consists of the anion BETA, the cation core NH₂, and five substituent groups (2 N_CH₂, 2 CH₃, and 1 OCH₂). The operating pressure in the absorber is 21.5 bar and the temperature in the flash tank is 334.9 K. The averaged CO_2 equilibrium solubility (molar fraction) in the absorber is as high as 0.458. In addition, the IL viscosity in the absorber is 10.3 mPa s. Comparing with most of the known ILs,[45] this value is quite small, resulting in a high CO_2 mass transfer coefficient.

In addition to the global optimal solution, the other top two ILs with their corresponding TACs are generated in Table 6. The three IL structures are similar. The anion and cation core in the three top ILs are BETA and NH₂, respectively. The involved two groups –OCH₂ and –OH are known to favor CO_2 absorption. With these top-ranked ILs, experimental verifications can be performed. This provides a larger probability of obtaining a reliable and optimal IL design in case that uncertainty is not considered.
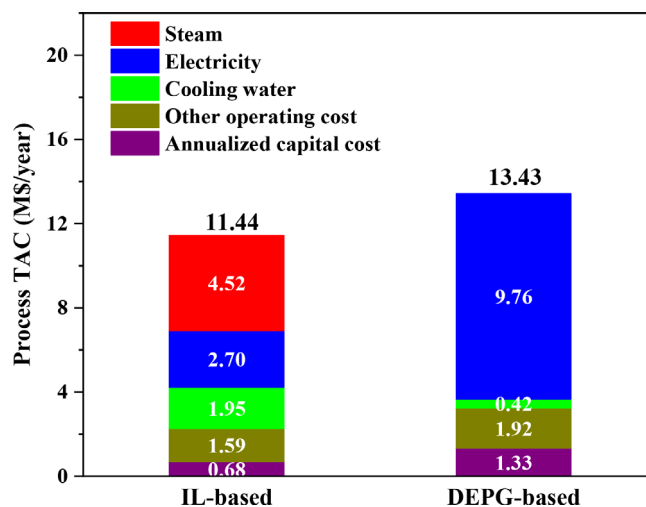
The DEPG-based Selexol process is widely used for pre-combustion carbon capture. As a benchmark, the economic performance of the Selexol process is evaluated. The flowsheet of the Selexol process is shown in Figure S1. It is simulated in Aspen Plus V8.8 according to literature reports[53,54] and the detailed process specifications are listed in Table S2. For consistency, the process economics is assessed with the same cost models used in this work. Figure 6 compares the cost breakdown of the two processes. As indicated, although a much larger amount of steam and cooling water are consumed in the IL-based

process, the electricity cost of the Selexol process is much higher than that of the IL-based process. This is because a higher pressure (30 bar) is needed in the absorber of the Selexol process to meet the CO_2 capture requirement, which leads to a larger electricity consumption for gas compressing. In contrast, our designed IL has a higher CO_2 solubility than DEPG, making the absorption operable at a lower pressure (21.5 bar). In total, the IL-based process can achieve 14.8% total cost reduction compared with the benchmark Selexol process for pre-combustion carbon capture, which demonstrates the significance and large benefit of integrated IL and process design.

6 | CONCLUSION

This article presents a new integrated IL and absorption process design approach for gas separation. The physical, kinetic, and thermodynamic properties of ILs are predicted by different types of methods (e.g., GC methods, empirical correlations, rigorous thermodynamic and data-driven models). In order to improve the reliability of the results, a rigorous rate-based absorption model, where both absorption thermodynamics and kinetics are incorporated, is used. With these, the integrated IL and process design task is formulated and solved as an MINLP optimization problem. The IL structure and process operating conditions are simultaneously optimized to minimize the total annualized cost. The proposed approach is demonstrated on a pre-combustion carbon capture example. In the case study, rigorous thermodynamic models (UNIFAC and PR) are first applied to predict the CO_2 equilibrium solubility in ILs, which results in a convergence failure of the MINLP problem. To tackle the problem, an ANN-based surrogate model is used to replace the thermodynamic models. Based on this, the integrated design problem is successfully solved to the global optimality. The result shows that compared with the DEPG-based Selexol process, the optimal IL-based process can achieve a better economic performance for the investigated carbon capture task.

To the best of our knowledge, this work is the first attempt in the global optimization of an integrated IL and process design problem where rigorous rate-based process model is employed. This study can be extended in several ways. For instance, the method can be applied to handle different CO_2 emission sources. In addition, the IL-based absorption process can be compared with other processes (e.g., adsorption and membrane) to identify the most efficient technology for gas separation problems. Despite the large progress, limitations should not be neglected. First, a simple inequality constraint is added to prevent unreasonable extrapolation of the ANN-based solubility model. In the future work, more advanced methods (e.g., convex hull[55] and topological data analysis[56]) can be used to confine the results into the validity region. Second, the current work cannot distinguish between structural isomers. To do so, higher-order GC models incorporating the group connectivity information are required, which may significantly increase the computational demand. A more realistic strategy is to investigate the practical performance of isomers in a post-design step, for example, by experimental studies. Thirdly, the uncertainty associated with property prediction can directly affect the quality of the optimal design. This issue is worth to be explicitly considered in the computer-aided design stage for better reliability. Efforts in these directions are underway.

AUTHOR CONTRIBUTIONS

Xiang Zhang: Investigation; writing-original draft. **Xuechong Ding:** Data curation; software. **Zhen Song:** Validation. **Teng Zhou:** Methodology; supervision; writing-review & editing. **Kai Sundmacher:** Methodology; resources.

DATA AVAILABILITY STATEMENT

The data that support the findings of this study are available from the corresponding author upon reasonable request.

ORCID

Teng Zhou https://orcid.org/0000-0003-1941-5348
Kai Sundmacher https://orcid.org/0000-0003-3251-0593

REFERENCES

1. Eimer D. *Gas Treating: Absorption Theory and Practice*. United Kingdom: John Wiley & Sons; 2014.
2. Papadopoulos AI, Badr S, Chremos A, et al. Computer-aided molecular design and selection of CO_2 capture solvents based on thermodynamics, reactivity and sustainability. *Mol Syst Des Eng*. 2016;1(3):313-334.
3. Ramdin M, de Loos TW, Vlugt TJH. State-of-the-art of CO_2 capture with ionic liquids. *Ind Eng Chem Res*. 2012;51(24):8149-8177.
4. Zhang X, Zhang X, Dong H, Zhao Z, Zhang S, Huang Y. Carbon capture with ionic liquids: overview and progress. *Energ Environ Sci*. 2012;5(5):6668-6681.
5. Wang J, Song Z, Cheng H, Chen L, Deng L, Qi Z. Computer-aided design of ionic liquids as absorbent for gas separation exemplified by CO_2 capture cases. *ACS Sustain Chem Eng*. 2018;6(9):12025-12035.
6. Zhang X, Liu Z, Wang W. Screening of ionic liquids to capture CO_2 by COSMO-RS and experiments. *AIChE J*. 2008;54(10):2717-2728.
7. Song Z, Zhou T, Zhang J, Cheng H, Chen L, Qi Z. Screening of ionic liquids for solvent-sensitive extraction –with deep desulfurization as an example. *Chem Eng Sci*. 2015;129:69-77.
8. Zhao Y, Gani R, Afzal RM, Zhang X, Zhang S. Ionic liquids for absorption and separation of gases: an extensive database and a systematic screening method. *AIChE J*. 2017;63(4):1353-1367.
9. Mortazavi-Manesh S, Satyro MA, Marriott RA. Screening ionic liquids as candidates for separation of acid gases: solubility of hydrogen sulfide, methane, and ethane. *AIChE J*. 2013;59(8):2993-3005.
10. Wang Y, Achenie LEK. Computer aided solvent design for extractive fermentation. *Fluid Phase Equilib*. 2002;201(1):1-18.
11. Karunanithi AT, Achenie LEK, Gani R. A new decomposition-based computer-aided molecular/mixture design methodology for the design of optimal solvents and solvent mixtures. *Ind Eng Chem Res*. 2005;44(13):4785-4797.
12. Karunanithi AT, Achenie LEK, Gani R. A computer-aided molecular design framework for crystallization solvent design. *Chem Eng Sci*. 2006;61(4):1247-1260.

13. Austin ND, Sahinidis NV, Trahan DW. Computer-aided molecular design: an introduction and review of tools, applications, and solution techniques. *Chem Eng Res Des*. 2016;116:2-26.

14. Chávez-Islas LM, Vasquez-Medrano R, Flores-Tlacuahuac A. Optimal molecular design of ionic liquids for high-purity bioethanol production. *Ind Eng Chem Res*. 2011;50(9):5153-5168.

15. Chen Y, Koumaditi E, Gani R, Kontogeorgis GM, Woodley JM. Computer-aided design of ionic liquids for hybrid process schemes. *Comput Chem Eng*. 2019;130:106556.

16. Liu X, Chen Y, Zeng S, et al. Structure optimization of tailored ionic liquids and process simulation for shale gas separation. *AIChE J*. 2020; 66(2):e16794.

17. Karunanithi AT, Mehrkesh A. Computer-aided design of tailor-made ionic liquids. *AIChE J*. 2013;59(12):4627-4640.

18. Chong FK, Foo DCY, Eljack FT, Atilhan M, Chemmangattuvalappil NG. Ionic liquid design for enhanced carbon dioxide capture by computer-aided molecular design approach. *Clean Technol Environ Policy*. 2015;17 (5):1301-1312.

19. Chong FK, Eljack FT, Atilhan M, Foo DCY, Chemmangattuvalappil NG. A systematic visual methodology to design ionic liquids and ionic liquid mixtures: green solvent alternative for carbon capture. *Comput Chem Eng*. 2016;91:219-232.

20. Song Z, Zhang C, Qi Z, Zhou T, Sundmacher K. Computer-aided design of ionic liquids as solvents for extractive desulfurization. *AIChE J*. 2018;64(3):1013-1025.

21. Lei Z, Dai C, Liu X, Xiao L, Chen B. Extension of the UNIFAC model for ionic liquids. *Ind Eng Chem Res*. 2012;51(37):12135-12144.

22. Lei Z, Dai C, Wang W, Chen B. UNIFAC model for ionic liquid-CO_2 systems. *AIChE J*. 2014;60(2):716-729.

23. Song Z, Zhou T, Qi Z, Sundmacher K. Extending the UNIFAC model for ionic liquid–solute systems by combining experimental and computational databases. *AIChE J*. 2020;66(2):e16821.

24. Zhou T, Shi H, Ding X, Zhou Y. Thermodynamic modeling and rational design of ionic liquids for pre-combustion carbon capture. *Chem Eng Sci*. 2021;229:116076.

25. Stavrou M, Lampe M, Bardow A, Gross J. Continuous molecular targeting–computer-aided molecular design (CoMT–CAMD) for simultaneous process and solvent design for CO_2 capture. *Ind Eng Chem Res*. 2014;53(46):18029-18041.

26. Chong FK, Foo DCY, Eljack FT, Atilhan M, Chemmangattuvalappil NG. A systematic approach to design task-specific ionic liquids and their optimal operating conditions. *Mol Syst Des Eng*. 2016;1(1):109-121.

27. Dong K, Liu X, Dong H, Zhang X, Zhang S. Multiscale studies on ionic liquids. *Chem Rev*. 2017;117(10):6636-6695.

28. Burger J, Papaioannou V, Gopinath S, Jackson G, Galindo A, Adjiman CS. A hierarchical method to integrated solvent and process design of physical CO_2 absorption using the SAFT-γ Mie approach. *AIChE J*. 2015;61(10):3249-3269.

29. Valencia-Marquez D, Flores-Tlacuahuac A, Vasquez-Medrano R. An optimization approach for CO_2 capture using ionic liquids. *J Clean Prod*. 2017;168:1652-1667.

30. Zhou T, Zhou Y, Sundmacher K. A hybrid stochastic–deterministic optimization approach for integrated solvent and process design. *Chem Eng Sci*. 2017;159:207-216.

31. Pereira FE, Keskes E, Galindo A, Jackson G, Adjiman CS. Integrated solvent and process design using a SAFT-VR thermodynamic description: high-pressure separation of carbon dioxide and methane. *Comput Chem Eng*. 2011;35(3):474-491.

32. de Riva J, Suarez-Reyes J, Moreno D, Díaz I, Ferro V, Palomar J. Ionic liquids for post-combustion CO_2 capture by physical absorption: thermodynamic, kinetic and process analysis. *Int J Greenh Gas Control*. 2017;61:61-70.

33. Mota-Martinez MT, Brandl P, Hallett JP, Mac DN. Challenges and opportunities for the utilisation of ionic liquids as solvents for CO_2 capture. *Mol Syst Des Eng*. 2018;3(3):560-571.

34. Palomar J, Larriba M, Lemus J, et al. Demonstrating the key role of kinetics over thermodynamics in the selection of ionic liquids for CO_2 physical absorption. *Sep Purif Technol*. 2019;213:578-586.

35. Seo K, Tsay C, Hong B, Edgar TF, Stadtherr MA, Baldea M. Rate-based process optimization and sensitivity analysis for ionic-liquid-based post-combustion carbon capture. *ACS Sustain Chem Eng*. 2020; 8(27):10242-10258.

36. Samudra AP, Sahinidis NV. Optimization-based framework for computer-aided molecular design. *AIChE J*. 2013;59(10):3686-3701.

37. Schweidtmann AM, Huster WR, Lüthje JT, Mitsos A. Deterministic global process optimization: accurate (single-species) properties via artificial neural networks. *Comput Chem Eng*. 2019;121:67-74.

38. Huster WR, Schweidtmann AM, Lüthje JT, Mitsos A. Deterministic global superstructure-based optimization of an organic rankine cycle. *Comput Chem Eng*. 2020;141:106996.

39. Lei Z, Dai C, Chen B. Gas solubility in ionic liquids. *Chem Rev*. 2014; 114(2):1289-1326.

40. Chen Y, Gani R, Kontogeorgis GM, Woodley JM. Integrated ionic liquid and process design involving azeotropic separation processes. *Chem Eng Sci*. 2019;203:402-414.

41. Churi N, Achenie LEK. Novel mathematical programming model for computer aided molecular design. *Ind Eng Chem Res*. 1996;35 (10):3788-3794.

42. Lazzús JA. A group contribution method to predict the melting point of ionic liquids. *Fluid Phase Equilib*. 2012;313:1-6.

43. Huang Y, Dong H, Zhang X, Li C, Zhang S. A new fragment contribution-corresponding states method for physicochemical properties prediction of ionic liquids. *AIChE J*. 2013;59(4):1348-1359.

44. Paduszyński K, Domańska U. A new group contribution method for prediction of density of pure ionic liquids over a wide range of temperature and pressure. *Ind Eng Chem Res*. 2012;51(1):591-604.

45. Paduszyński K, Domańska U. Viscosity of ionic liquids: an extensive database and a new group contribution model based on a feed-forward artificial neural network. *J Chem Inf Model*. 2014;54(5):1311-1324.

46. Paulechka YU, Kabo AG, Blokhin AV, Kabo GJ, Shevelyova MP. Heat capacity of ionic liquids: experimental determination and correlations with molar volume. *J Chem Eng Data*. 2010;55(8):2719-2724.

47. Dvorak BI, Lawler DF, Fair JR, Handler NE. Evaluation of the Onda correlations for mass transfer with large random packings. *Environ Sci Technol*. 1996;30(3):945-953.

48. Mota-Martinez MT, Hallett JP, Mac DN. Solvent selection and design for CO_2 capture – how we might have been missing the point. *Sustain Energy Fuels*. 2017;1(10):2078-2090.

49. Song Z, Shi H, Zhang X, Zhou T. Prediction of CO_2 solubility in ionic liquids using machine learning methods. *Chem Eng Sci*. 2020;223: 115752.

50. Carvalho PJ, Coutinho JAP. On the nonideality of CO_2 solutions in ionic liquids and other low volatile solvents. *J Phys Chem Lett*. 2010;1 (4):774-780.

51. Couper JR, Penney WR, Fair JR, Walas SM. *Chemical Process Equipment: Selection and Design (Revised Second Edition)*. Boston: Gulf Professional Publishing; 2009.

52. Kılınç MR, Sahinidis NV. Exploiting integrality in the global optimization of mixed-integer nonlinear programming problems with BARON. *Optim Methods Softw*. 2018;33(3):540-562.

53. Im D, Roh K, Kim J, Eom Y, Lee JH. Economic assessment and optimization of the Selexol process with novel additives. *Int J Greenh Gas Control*. 2015;42:109-116.

54. Zhang X, Song Z, Gani R, Zhou T. Comparative economic analysis of physical, chemical, and hybrid absorption processes for carbon capture. *Ind Eng Chem Res*. 2020;59(5):2005-2012.

55. Kahrs O, Marquardt W. The validity domain of hybrid models and its application in process optimization. *Chem Eng Process*. 2007;46(11): 1054-1066.

56. Schweidtmann AM, Weber JM, Wende C, Netze L, Mitsos A. Obey validity limits of data-driven models. *arXiv Preprint*. 2020. https://arxiv.org/abs/2010.03405.

SUPPORTING INFORMATION

Additional supporting information may be found online in the Supporting Information section at the end of this article.